Electron capture in GaAs quantum wells

Paul Sotirelis and Karl Hess
Beckman Institute, University of Illinois at Urbana-Champaign, Urbana, Illinois 61801
(Received 4 October 1993)

The capture time for an electron in a graded index separate confinement heterostructure (GRINSCH) is calculated as a function of quantum-well width. The electron's interactions with the other electrons in the well along with the phonons are included in the random-phase approximation using full multiple-subband and frequency-dependent screening. It is shown that at sufficiently high electron densities, there is a significant increase of the capture rate with electron density except for quantum-well widths near a phonon resonance.

I. INTRODUCTION

The capture time of electrons and holes in semiconductor quantum-well heterostructures is currently of great interest. This interest is being driven by efforts to optimize the device characteristics of quantum-well lasers, particularly the modulation bandwidth. Investigations attempting to predict the carrier capture time through classical[1] or quantum mechanical methods[2] have met with only limited success,[3] until recently. Recent investigations of GaAs quantum-well structures have succeeded in confirming some quantum mechanical aspects of electron capture and have identified LO-phonon emission as the primary scattering mechanism.[4–8] In addition, one of these investigations[4] predicts that electron capture due to electron-electron scattering, at sufficiently high electron densities, can be nearly as important as that due to LO-phonon emission. A separate study of intersubband scattering has confirmed the importance of electron-electron scattering at high electron densities.[9] In this paper we present an investigation of electron capture that includes the interactions of electrons in laser type geometries with the coupled electron-phonon system.

The highly inelastic nature of electron capture is ample motivation to include electron-electron scattering beyond the Thomas-Fermi approximation. In this work, scattering by inelastic electronic excitations is included in the random-phase approximation in conjunction with electron-phonon scattering through the use of full dynamic screening. Intersubband and intrasubband excitations (collective and pair) among all subbands are implicitly incorporated in our formulation. The screening of the phonons by the electrons and plasmon-phonon coupling are automatically included by considering electron-electron and electron-phonon (LO phonon) scattering in a consistent way such that they mutually interact and affect each other. Another benefit from our approach is the removal of the explicit dependence of the electron-electron interaction on the inverse screening length (as in the Thomas-Fermi approximation). Therefore, we avoid having to estimate this quantity.

A number of simplifying assumptions are made to facilitate the modeling of the heterostructure. The states of the electron are calculated in the effective mass approximation and the electrons are assumed to have the effective mass of the conduction band minimum for bulk GaAs. The wave functions and energies are determined from solving the Schrödinger equation, and band bending is neglected. The LO phonons are assumed to be bulk type, which has been shown to be a good overall approximation for carrier capture.[5]

In Sec. II, the details of the $Al_xGa_{1-x}As/GaAs$ P-GRINSCH type structure are given. The energies and wave functions of the subbands are numerically evaluated and discussed. In Sec. III the equations describing the capture time of an electron interacting with an equilibrium distribution of electrons and the lattice are presented. The capture rates are then evaluated and the results are discussed. Section IV contains a summary and some concluding remarks. All equations are given in cgs units.

II. QUANTUM-WELL STRUCTURE

We examine heterostructures corresponding to the P-GRINSCH laser (P—for parabolic grading) for various active layer widths. The active layer, the region of narrow confinement, is referred to as the quantum well. The much larger region surrounding the quantum-well is, as usual, referred to as the separate confinement region. The common characteristics of the heterostructures include a central GaAs quantum-well region, an $Al_xGa_{1-x}As$ ($x = 0.3$ to 0.6) separate confinement region, and an $Al_{0.6}Ga_{0.4}As$ outermost region. The quantum-well width is varied from 30 Å to 150 Å. The separate confinement region has a constant width of 4050 Å regardless of the quantum-well width. The discontinuities in the conduction band at the heterojunctions and the gradual change in the conduction band in the separate confinement region are calculated from the electron affinity and band gap of $Al_xGa_{1-x}As$.[10] All energies are relative to the conduction band minimum in the quantum-well region.

The electron wave functions and energies are calculated in the effective mass approximation where the z direction is chosen perpendicular to the heterojunction boundaries. This choice maintains translational invariance in the x-y directions and allows solutions of the form

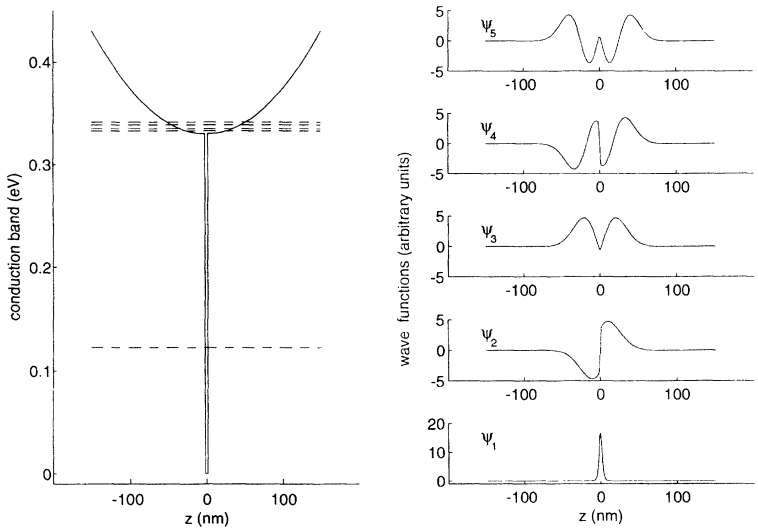

FIG. 1. The conduction band, subband energies, and wave functions are plotted versus the z axis (direction perpendicular to the active layer) for a quantum-well width of 30 Å.

$\Psi_{n\mathbf{k}}(\rho,z) = \frac{e^{i\mathbf{k}\cdot\rho}}{\sqrt{A}}\psi_n(z)$ and $E_{n\mathbf{k}} = E_n + \hbar^2k^2/2m^*$. The reduced Schrödinger equation is associated with the z direction and has the following form:

$$\left[\frac{-\hbar^2}{2m^*}\frac{d^2}{dz^2} + V(z)\right]\psi_n(z) = E_n\psi_n(z). \tag{1}$$

Band bending due to space charge accumulation is ignored. The effective mass m^* in the quantum well and separate confinement region is approximated by that of bulk GaAs and is given by $m^* = 0.067m_e$, where m_e is the free electron mass.

The subband wave functions and energies are then obtained by numerically solving Eq. (1) using the Numerov method.[11] Only the lowest five subbands are considered. The results are plotted for well widths of 30 Å, 82 Å, and 130 Å in Figs. 1, 2, and 3, respectively. For a quantum-well width of 30 Å, the ground state forms the only subband in the quantum well; the other subbands have closely spaced energy levels just above the conduction band discontinuity. For a quantum-well width of 82 Å, there are two subbands in the well and for a well width of 130 Å, there are four. Notice that the energy of the fifth subband changes very little with well width. In fact the energy of the fifth subband changes by only 2% over the entire range of well widths. Notice also that an electron in the fifth subband has a greater probability of being near the quantum well for a well width of 82 Å than for well widths of 30 Å and 130 Å. This point is important with regards to the overlap of the wave functions and the capture rate.

III. CAPTURE RATE

The relaxation rate of an electron in a multiple subband quantum well due to its interaction with a thermal distribution of electrons and phonons is given by[12]

$$\tau^{-1}_{\mathbf{k}i\to j} = \frac{2\pi}{\hbar}\frac{2}{(2\pi)^2}\int d^2q\ \frac{1}{2\pi}\mathrm{Im}\left[-V^{\mathrm{eff}}_{jiij}(\mathbf{q},\omega)\right] \times[1 - n_F(E_{i\mathbf{k}} - \hbar\omega) + n_b(\omega)]\ , \tag{2}$$

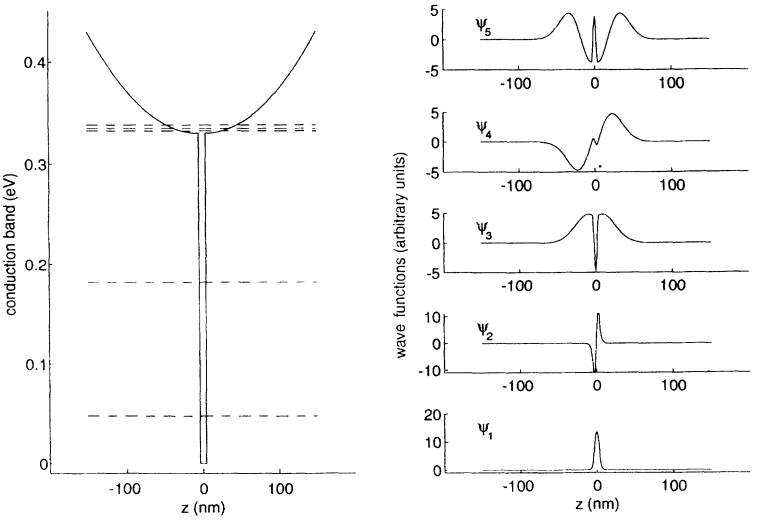

FIG. 2. The conduction band, subband energies, and wave functions are plotted versus the z axis (direction perpendicular to the active layer) for a quantum-well width of 82 Å.

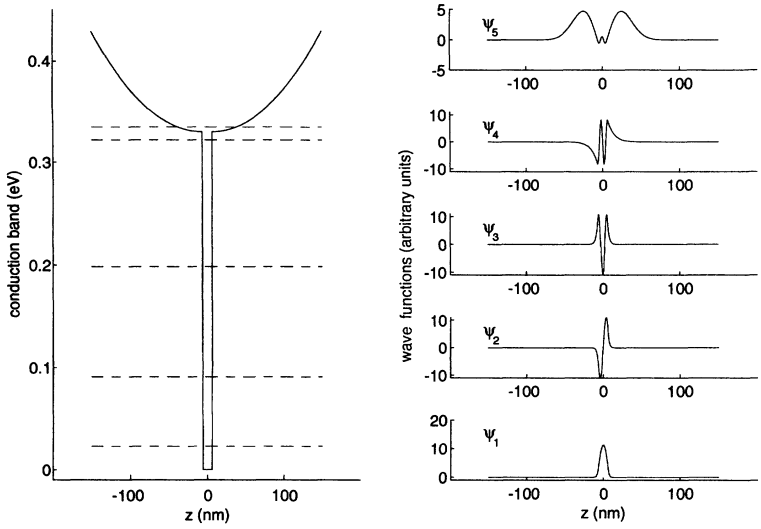

FIG. 3. The conduction band, subband energies, and wave functions are plotted versus the z axis (direction perpendicular to the active layer) for a quantum-well width of 130 Å.

where n_F is the Fermi-Dirac distribution, n_b is the Bose-Einstein distribution, $\hbar\omega = E_{i\mathbf{k}} - E_{j\mathbf{k}-\mathbf{q}}$, and $\mathbf{k}$ is the wave vector of the initial electron.

The matrix element $V^{\text{eff}}_{jiij}(\mathbf{q},\omega)$ is that of the screened interaction potential, and is determined from solving the following linear system:

$$V^{\text{Coul}}_{ijkl}(q) = \sum_{mn} \epsilon_{ijnm}(\mathbf{q},\omega) V^{\text{eff}}_{mnkl}(\mathbf{q},\omega) \ , \tag{3}$$

where $\epsilon_{ijnm}(\mathbf{q},\omega)$ is the frequency and wave-vector-dependent dielectric function and $V^{\text{Coul}}_{ijkl}(q)$ is the matrix element of the bare Coulomb potential. They are defined as follows:

$$\epsilon_{ijnm}(\mathbf{q},\omega) = \epsilon_{\text{latt}}(\omega)\delta_{im}\delta_{jn} - V^{\text{Coul}}_{ijnm}(q)\Pi^{\circ}_{mn}(\mathbf{q},\omega) \ , \tag{4}$$

$$\epsilon_{\text{latt}}(\omega) = \epsilon_{\infty} + \frac{(\epsilon_{\infty}-\epsilon_s)\omega_T^2}{,\omega^2 - \omega_T^2} \ , \tag{5}$$

$$\Pi^{\circ}_{mn}(\mathbf{q},\omega) = 2\sum_{\mathbf{k}} \frac{n_f(E_{m\mathbf{k}+\mathbf{q}}) - n_f(E_{n\mathbf{k}})}{E_{m\mathbf{k}+\mathbf{q}} - E_{n\mathbf{k}} - \hbar\omega - i\varepsilon} \ , \tag{6}$$

$$V^{\text{Coul}}_{ijnm}(q) = \frac{2\pi e^2}{q} \int\int dz_1\, dz_2\ \psi_i^*(z_1)\psi_j(z_1) \ , \times \exp(-q|z_1 - z_2|)\ \psi_m(z_2)\psi_n^*(z_2). \tag{7}$$

The low frequency dielectric function of GaAs $\epsilon_{\text{latt}}(\omega)$ assumes dispersionless bulk LO phonons, and a single oscillator model relating four parameters, the LO-phonon frequency ω_L, the TO-phonon frequency ω_T, the high frequency dielectric constant ϵ_∞, and the static dielectric constant ϵ_s.

Equation (2) is rewritten by transforming the variables of integration from (q,ϕ_q) to (q,ω). The resulting equation is given by

$$\tau^{-1}_{\mathbf{k}\,i\to j} = \frac{2\pi}{\hbar}\frac{2}{(2\pi)^2}\frac{2m}{\hbar k}\int dq \times \int d\omega \frac{\Theta[1-(q/2k + m\omega_{ji}/\hbar k q)^2]}{\sqrt{1-(q/2k+m\omega_{ji}/\hbar k q)^2}} \times \frac{1}{2\pi}\text{Im}\left[-V^{\text{eff}}_{jiij}(\mathbf{q},\omega)\right] \times [1 - n_f(E_{i\mathbf{k}} - \hbar\omega) + n_b(\omega)] \ , \tag{8}$$

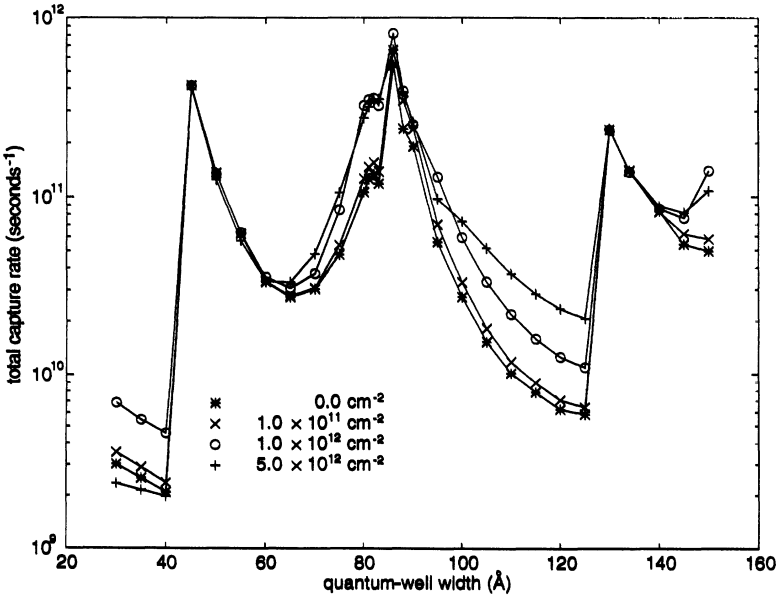

FIG. 4. The total capture rate is plotted versus quantum-well width for four electron densities. Asterisks correspond to zero density, crosses correspond to 10^{11} cm^{-2}, circles correspond to 10^{12} cm^{-2}, and pluses correspond to 5×10^{12} cm^{-2}.

where $\omega_{ji} = \omega + (E_j - E_i)/\hbar$ and $\Theta[x]$ is the step function (0 for $x < 0$ and 1 for $x > 0$). The region of integration is given by the region in (q, ω) space where the step function is nonzero.

We consider the capture of an electron from the fifth subband to all subbands with energy less than the conduction band discontinuity. The total capture rate is given by the sum of all possible transition rates. As an example, the total capture rate for the well width of 30 Å is $\tau_{5\to1}^{-1}$. However, the total capture rate for the well width of 130 Å is $\tau_{5\to1}^{-1} + \tau_{5\to2}^{-1} + \tau_{5\to3}^{-1} + \tau_{5\to4}^{-1}$. The initial electron energy is just under one LO-phonon energy above the subband edge for the entire range of well widths. This choice is consistent with the electrons in the separate confinement region quickly relaxing in energy by LO-phonon emission until near the active layer. For a quantum-well width of 30 Å, $E_{5\mathbf{k}} = 0.37554$ eV, $E_5 = 0.3414$ eV, and $E_5 + \hbar\omega_L = 0.37813$ eV. For a quantum-well width of 150 Å, $E_{5\mathbf{k}} = 0.36806$ eV, $E_5 = 0.3346$ eV, and $E_5 + \hbar\omega_L = 0.37133$ eV. We evaluate the capture time at zero temperature only to save cpu time.[13]

The total capture rate is plotted versus well width for four different densities in Fig. 4. Certain features can be explained by considering zero electron density (only polar-optical phonon scattering). The abrupt increases in the capture rate with increasing well width correspond to when the energy of a given subband falls below the top of the conduction band discontinuity, and therefore can be considered "bound" in the well. This happens approximately at 45 Å, 85 Å, and 125 Å, for the second, third, and fourth subbands, respectively. In Fig. 5, we choose to plot the zero density transition rates versus well width individually (i.e., $\tau_{5\to1}^{-1}, \tau_{5\to2}^{-1}, \tau_{5\to3}^{-1}, \tau_{5\to4}^{-1}$). It is apparent that the transition rates for the newly bound subbands decrease from a local maximum with increasing well width. This is due to the $1/q$ dependence of the Fröhlich Hamiltonian which favors transitions for which the energy separation of the subbands is close to the LO-phonon energy. This is commonly referred to as the phonon resonance. A second trend that is seen in Fig. 5 is that the rates exhibit a common peak around 82 Å as well as troughs around 30 Å and 130 Å. This resonance is due to the overlap of the wave functions of the initial (fifth) and final subband. This is verified by Figs. 1–3 showing that an electron in the fifth subband has a much greater probability of being in the quantum-well region if the well width is 82 Å as compared to well widths of 30 Å and 130 Å. This type of peak is commonly referred to as an overlap resonance.

The four densities considered in Fig. 4 are zero, 10^{11} cm^{-2}, 10^{12} cm^{-2}, and 5×10^{12} cm^{-2}. There is little difference in the capture rate corresponding to the lowest density, 10^{11} cm^{-2}, and that corresponding to zero density. The capture rate for the two highest densities, 10^{12} cm^{-2}, and 5×10^{12} cm^{-2}, are shown to be significantly greater than the zero density rate for many well widths.[14] The inclusion of electron-electron scattering is shown to have the least effect for well widths corresponding to phonon resonances. This is especially obvious from Fig. 6, where the transition rate from subband 5 to subband 2 is plotted. However, it is also very apparent that away from the phonon resonance, the transition rate can be up to 6 times the zero density rate. Therefore, electron-electron scattering, at high electron densities, sets a limit to long electron-phonon capture times.

In the most recent experiments and in typical laser operation, there is a distribution of electrons competing to be captured. The averaging over the initial states is important for the comparison between experiment and theory. However, we have not performed such an average due to the large cpu times per data point. Certain qualitative effects can be expected if such an average was performed. The sharpness of the phonon resonances will be broadened due to electrons occupying different energies within the initial subband (5). The states in other subbands will also contribute. An electron in subband

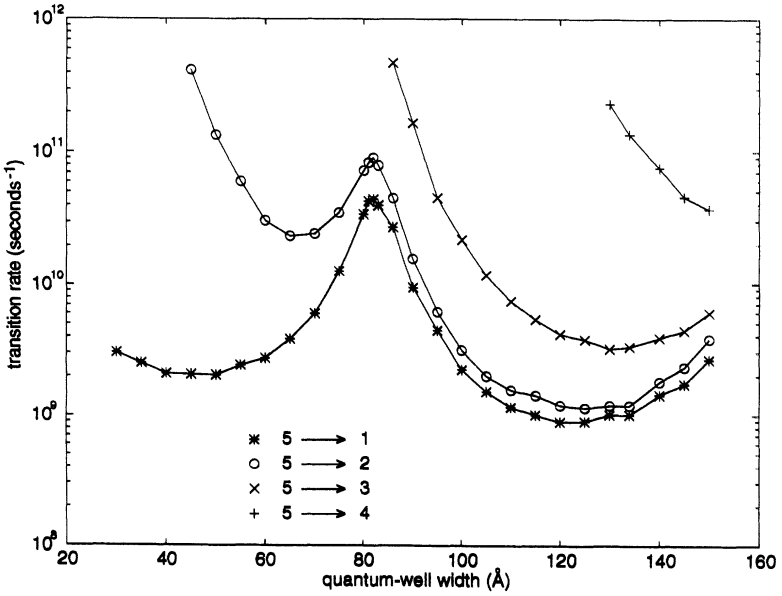

FIG. 5. The separate transition rates from one subband to another at zero density are plotted. Asterisks correspond to the five to one transition, circles correspond to the five to two transition, crosses correspond to the five to three transition, and pluses correspond to the five to four transition.

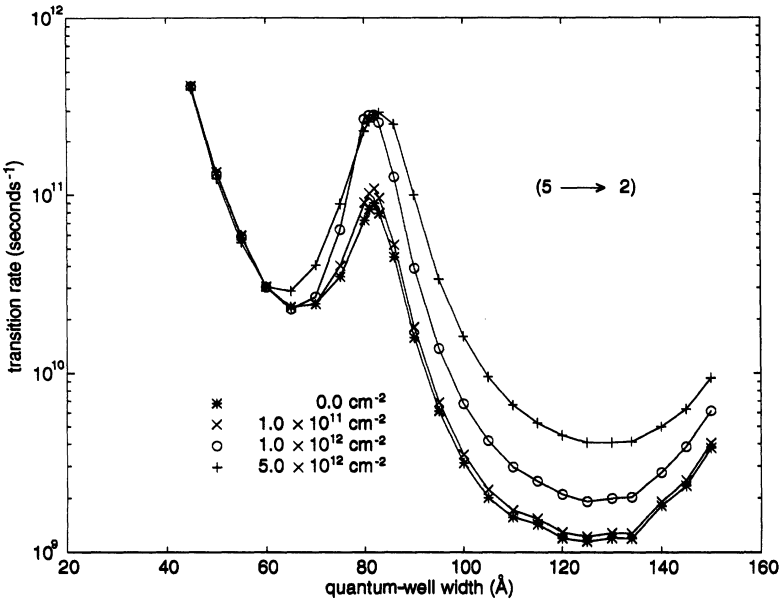

FIG. 6. The transition rate from subband five to subband two is plotted versus quantum-well width for four electron densities. Asterisks correspond to zero density, crosses correspond to 10^{11} cm^{-2}, circles correspond to 10^{12} cm^{-2}, and pluses correspond to 5×10^{12} cm^{-2}.

four has an optimal (minimal) probability of being in the quantum-well region for a well width of 30 Å (82 Å). This is exactly opposite of subband five, and an average over these states would tend to increase the capture rates for well widths where the rate is at its very lowest. Therefore in addition to electron-electron scattering, averaging over different initial subband states also will limit extremely long capture times and reduce the variation of the capture time versus well width.

IV. CONCLUSION

The capture time of an electron in a P-GRINSCH type heterostructure has been calculated versus well width, assuming a finite electron density in the well. Electron-electron and electron-phonon (bulk LO-phonon) scattering mechanisms are included in the random-phase approximation using full multiple-subband and frequency-dependent screening. At sufficiently high electron densities, there is a significant increase of the capture rate for well widths away from the phonon resonance. Since typical laser operation involves relatively high electron densities, the importance of electron-electron scattering should not be overlooked in the study of the carrier capture process.

ACKNOWLEDGMENTS

We acknowledge support from the NSF Center for Compound Microelectronics and the Office of Naval Research.

[1] H. Shichijo, R. M. Kolbas, N. Holonyak, R. D. Dupuis, and P. D. Dapkus, Solid State Commun. **27**, 1029 (1978); J. Y. Tang, K. Hess, N. Holonyak, J. J. Coleman, and P. D. Dapkus, J. Appl. Phys. **53**, 6043 (1982).

[2] J. A. Brum and G. Bastard, Phys. Rev. B **33**, 1420 (1986); J. A. Brum, T. Weil, J. Nagle, and B. Vinter, *ibid.* **34**, 2381 (1986); S. V. Kozyrev and A. Y. Shik, Fiz. Tekh. Poluprovodn. **19**, 1667 (1985) [Sov. Phys. Semicond. **19**, 1024 (1985)].

[3] D. Y. Oberli, J. Shah, J. L. Jewell, and T. C. Damen, Appl. Phys. Lett. **54**, 1028 (1989); B. Deveaud, J. Shah, T. C. Damen, and W. T. Tsang, Appl. Phys. Lett. **52**, 1886 (1988).

[4] P. W. M. Blom, J. E. M. Haverkort, P. J. van Hall, and J. H. Wolter, Appl. Phys. Lett. **62**, 1490 (1993).

[5] P. W. M. Blom, C. Smit, J. E. M. Haverkort, and J. H. Wolter, Phys. Rev. B **47**, 2072 (1993).

[6] B. Deveaud, A. Chomette, D. Morris, and A. Regreny, Solid State Commun. **85**, 367 (1993).

[7] M. R. X. Barros, P. C. Becker, D. Morris, B. Deveaud, and A. Regreny, Phys. Rev. B **47**, 10 951 (1993).

[8] D. Morris, B. Deveaud, A. Regreny, and P. Auvray, Phys. Rev. B **47**, 6819 (1993).

[9] P. Sotirelis, P. von Allmen, and K. Hess, Phys. Rev. B **47**, 12 744 (1993).

[10] S. Adachi, J. Appl. Phys. **58**, R1 (1985).

[11] P. C. Chow, Amer. J. Phys. **40**, 730 (1972).

[12] The derivation of the transition rate and explanations of the related equations are found in Ref. 9 and the references cited therein.

[13] The speed up occurs from the analytic evaluation of Eq. (6) at zero temperature.

[14] The transition rate is expected to increase monotonically with density, reach a maximum, and then monotonically decrease. This behavior is predicted on the basis of the results of Ref. 9, and is generally true for initial subbands well above the chemical potential. Therefore the capture rate for the highest density is less than the rate corresponding to lower densities for some well widths.